Influence of Metal Nitrates on the Structural and Magnetic Properties of Zinc ferrite Nanoparticles prepared by Sol-Gel Technique

Rosna[1], T Raguram[2] and K S Rajni[2]*

[1]Department of Physics, Farook Arts and Science College, Kottakkal (P.O),
Malappuram-676503, Kerala

[2]Dept. of Sciences, Amrita School of Engineering, Coimbatore,
Amrita Vishwa Vidyapeetham, India
Ks_rajani@cb.amrita.edu

Abstract

In the present work, ZnFe2O4 nanoparticles are prepared by varying the concentration of citric acid (CA) to metal nitrate (MN) ratio as 0.8, 0.6 and 0.4 by sol-gel technique. Structural analysis by XRD shows the cubic face of the normal spinal ferrite structure and the planes matches with the JCPDS data. The microstructural calculations show the decrease in grain size with decrease in the CA/MN ratio from 0.8, to 0.4. The stress and the dislocation density depend on the average crystallite size and it increases with a decrease in the crystallite size. The X-ray density increases with a decrease in the lattice constant. The ionic radius at the tetrahedral and octahedral sites varies as the CA/MN ratio varies. The presence of functional group is confirmed by FTIR analysis and the absence of the additional peak shows the purity of the prepared samples. The intrinsic stretching vibrations of Fe-O bonds observed at 550 cm^{-1} and the vibrations of octahedral complexes Zn-O are observed at 410 cm^{-1}. The morphology observed by SEM shows the spherical size particle with agglomeration at some regions and pores observed in the SEM micrograph is due to the evolution of gases during the synthesis process. The magnetic studies show the increase in the saturation magnetization with variation in the crystallite size is attributed to the superexchange interaction between the atom in the tetrahedral and octahedral sites. The coercivity and the remanence increases with the crystallite size. The observed remanence ratio Mr/Ms, which is the direction of magnetization after the magnetic field switch, varies with the crystallite size.

Keywords: ZnFe, Structural, FTIR, SEM with EDS and VSM

1. Introduction

The materials in its nano regime are given more importance in the technological applications due to its unique properties such as electrical conductivity, optical bandgap, refractive index, magnetic properties, mechanical properties such as hardness and chemical properties compared to their bulk counterpart [1]. Spinel ferrites are magnetic materials and they are popular due to its applications in electronic ignition systems, generators, medical implants, transformer circuits magnetic sensors and recording equipment, telecommunications, magnetic fluids, microwave absorbers and other high-frequency applications [2-5]. The major difference between ferrite with other magnetic materials such as iron and metallic alloys are its higher electrical resistivity which leads to better performance at higher frequencies. This property prevents induction of eddy currents and hence the loss of energy. Also, high permeability and temperature stability are the other advantages [6]. In addition, the ferrites are economically viable and the properties can be tuned by the synthesis process to specific applications. Among the spinal ferrites, zinc ferrite is a normal ferrite with FCC structure and has molecular formula MFe_2O_4, where M = Ni, Co, Mn, Zn, etc. Bulk Zinc ferrite has normal ferrite structure with Zn^{2+} ions occupy the tetrahedral sites and Fe^{3+} ions occupy the octahedral sites, In nano-regime zinc ferrites, shows partial inverse spinal structure is observed in which the divalent cation distribution is based on the formula $[Zn^{2+}_{1-\delta}Fe^{3+}_{\delta}]$ $[Zn^{2+}_{\delta}$ $Fe^{3+}_{2-\delta}]O^{2-}_{4}$ where δ is the inversion coefficient which is defined as the fraction of the tetrahedral site occupied by Fe^{3+}cations and it depends on the crystallite size and method of preparation [7,8]. Zinc ferrites possess unique magnetic, magneto-optical, magneto-resistive, thermal, electric, and mechanical properties [9-11]. It has wide variety applications such as magnetic materials [12, 13], gas sensor [14], catalysts [15], photocatalysts [16], absorbent materials [7, 17, 18] and so on. Zinc ferrite nanoparticle can be prepared by ball milling [19], sol-gel [20], co-precipitation [21], hydrothermal [22], auto-combustion route [23], and ultrasonic cavitation [24]. In the present work, nickel ferrite nanoparticles are prepared by sol-gel technique using citric acid as the chelating agent.

2. Experimental

2.1 Synthesis of Zinc Ferrite Nanoparticle

0.2 M zinc nitrate $[Zn(NO_3)_2\ 6H_2O]$ and 0.3M ferric nitrate $[\ Fe\ (NO_3)_3\ 9H_2O]$ and 0.4 M citric acid $[C_7H_8O_7.H_2O]$ is prepared in distilled water separately and the concentration of CA/MN ratio is taken as 0.8, 0.6 and 0.4. The pH of the solution is maintained at 8 using ammonia. The mixed solution is then heated to 80°C with constant stirring for two hours till a brown gel is obtained. The gel is heated to 800°C for three hours to remove excess water. The final product, the fluffy mass is grinded to get nanopowder.

2.2 Characterization

The samples are subjected to Powder X-ray diffraction analysis using Shimadzu XRD 6000 diffractometer with a CuKα radiation of wavelength of 1.541 Å.

The crystallite size (D) is calculated using the Scherrer formula [25] from the full- width at half maximum (FWHM)(β) for the most intense peak (311)

$D= (k\ \lambda) / (\beta\ \cos\theta)$ A°

In general, diffraction peak from a lattice plane is labeled as Miller indices (h, k, l) and these indices are related to inter-atomic spacing (d) spacing. For Cubic crystals, the lattice parameter ‘a’ is calculated using the relation [25]

a = dhkl /(h2 + k2 + l2)1/2 Å

The strain (ε) is calculated from the relation with β

$\varepsilon = \beta\ \cos\theta / 4$

The dislocation density (ρ) is defined as the length of dislocation lines per unit volume of the crystal, is calculated from the formula

$\rho=1/D^2$ (lines /cm^3)

The theoretical X-ray density,(ρx) is calculated by the relation [26]

$\rho_x =8M/Na^3$ (g/cm^3)

Where M is the molecular weight of the sample and A is the Avogadro’s number ($6.022\times10^{23}mol^{-1}$) and ‘a’ is the lattice parameter

X-ray diffraction data is further used to calculate ionic radii (rA, rB) and bond lengths (A-O), (B-O) at the tetrahedral and octahedral sites, are calculated by the equations.

$r_A = (u-\frac{1}{4})a\sqrt{3} - r(O^{-2})$ Å

$r_B = (\frac{5}{8}-u)a - r(O^{-2})$ Å

$A\text{-}O = (u-\frac{1}{4})a\sqrt{3}$ Å

$B\text{-}O = (\frac{5}{8}-u)a$ Å

Where a is the lattice constant; r (O^{-2}) is the radius of oxygen ion (1.35 Å); u is the oxygen ion parameter, for ideal spinel ferrite u=3/8.

Hopping lengths at tetrahedral sites (L_A) and octahedral sites (L_B) which is the distance between the magnetic ions is calculated by the following equation

$L_A = a(\sqrt{\frac{3}{4}})$ Å

$L_B = a(\sqrt{\frac{2}{4}})$ Å

The functional group is analyzed by FTIR using Perkin-Elmer spectrometer by KBr pellet technique in the range of 4000-400 cm^{-1}. The morphology and elemental analysis of the prepared samples are assessed by Scanning Electron microscopy with EDAX using JEOL (JSM 6390). The magnetic parameters are analyzed by Vibrating sample magnetometer (cryogenic, UK).

3. Results and Discussion

3.1 Structural Analysis

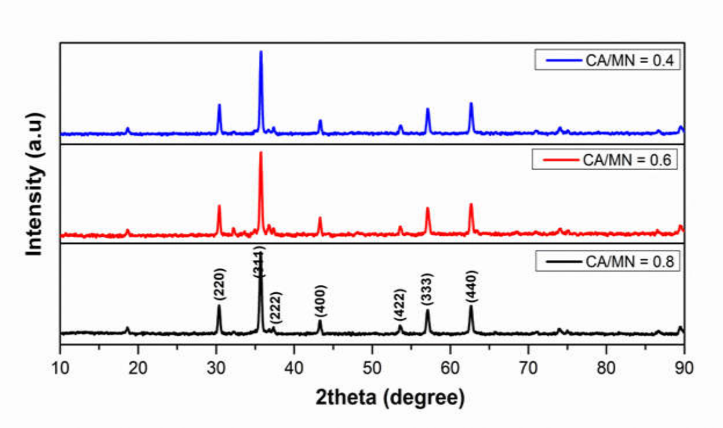

Figure 1. PXRD pattern of Zinc ferrite nanoparticles prepared at different CA/MN ratio

Figure 1 shows the X-ray diffraction pattern of the $ZnFe_2O_4$ nanoparticle prepared at different CA/MN ratio. The diffraction peaks at the plane (220), (311), (222), (400), (422), (333) and (440) are consistent with the pure spinal phase of the $ZnFe_2O_4$ nanoparticles. [JCPDS data (card no 22-1012)] [27]. It is noted that for all the samples the peaks are sharper with higher intensity shows the improved crystallinity of the synthesized particle. The sharpness of the peaks is the good indicator for the crystallinity [28, 29] and in the present case it is due to the complete conversion of unreacted oxides by citric acid which acts as a fuel and it results in improved crystallinity. The calculated strain and dislocation density varies as the average grain size varies. X-ray density depends on the lattice constant and molecular weight of the material. In the present case, X-ray density increases with a decrease in the lattice constant. The reverse is noted by Pandit et al for Mg-Zn ferrite system prepared at different molar concentrations [30]. The increase in the X-ray density with the decrease in CA/MN ratio is due to the formation of pores during the synthesis process [31] and also due to the ionic radii [32]. The mean ionic radius at the tetrahedral site A (rA) is found to decrease slowly with the octahedral site B (rB). The hopping length at the tetrahedral site (LA) and octahedral site (LB) decreases gradually when the CA/MN ratio changes from 0.8 to 0.4. The calculated bond length A-O and B-O found to decrease which reflects the decrease in lattice constant.

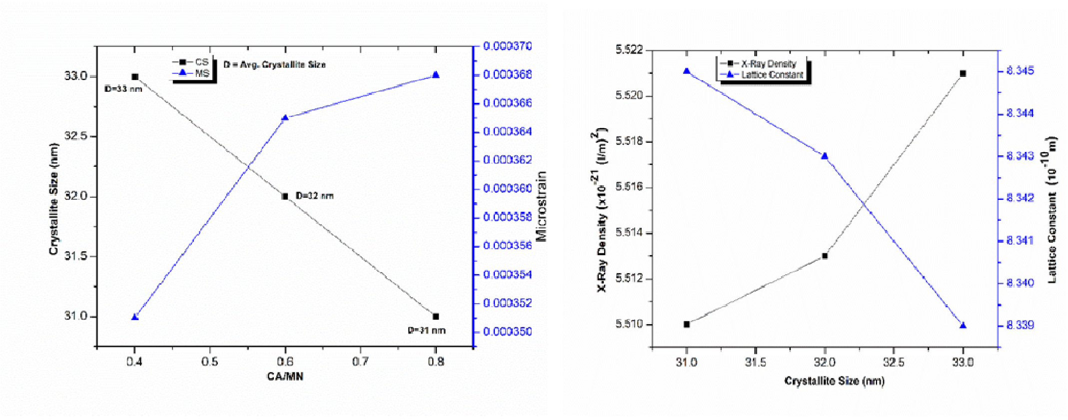

a) **b)**

Figure 2. a) Crystallite Size Vs Microstrain Vs CA/MN and b) X-Ray Density VS Lattice Constant Vs Crystallite size of Zinc ferrite nanoparticles prepared at different CA/MN ratio

Table 1. Microstructural analysis of Zinc ferrite nanoparticle prepared at different CA/MN ratio

CA/MN ratio	Lattice Constant a (Å)	L_A(Å)	L_B(Å)	A-O (Å)	B-O (Å)	tetrahedral ion radii (r_A)(x10^{-11}m)	octahedral ion radii (r_B) (x10^{-11}m)
0.8	8.341	3.129	2.950	1.8059	2.0853	4.559	7.353
0.6	8.339	3.128	2.949	1.8055	2.0848	4.555	7.348
0.4	8.335	3.127	2.948	1.8047	2.0839	4.547	7.339

3.2 Functional Group Analysis

FT-IR spectrum is used to collect information about the structure of a compound. It is noted that nitrate group has six normal vibrations that are IR active and found in IR spectra [33]. Figure 3 shows the FTIR Spectra of ZnFe2O4 nanoparticles at different CA/MN ratio. The FT-IR spectrum for the synthesized zinc ferrite nanoparticle show peaks at 3410, 1630, 550 and 410cm^{-1}. For pure zinc ferrite nanoparticle, the absorption bands observed at 410 and 550cm^{-1} which indicate the formation of pure zinc ferrite material [34]. The absence of peaks in the range 1000-1300 cm^{-1} and 2000-3000 cm^{-1}

show the nonexistence of O-H, C-O and C=H stretching mode of organic sources [35]. This result confirms that the material prepared at higher temperature remove the unwanted impurities during the preparation process. The band around 3410cm^{-1} and 1630 cm^{-1} correspond to the stretching modes and H-O-H bending vibrations of free or absorbed water. The intrinsic stretching vibrations of metal at the tetrahedral sites was observed around 540cm^{-1} which is the characteristics of the spinal ferrites [36]. This result is agreement with Waldron [37] in which the higher frequency bands (550 cm^{-1}) assigned to the tetrahedral group Fe – O and the low-frequency bands (410 cm^{-1}) to the octahedral group, Zn-O bonds.

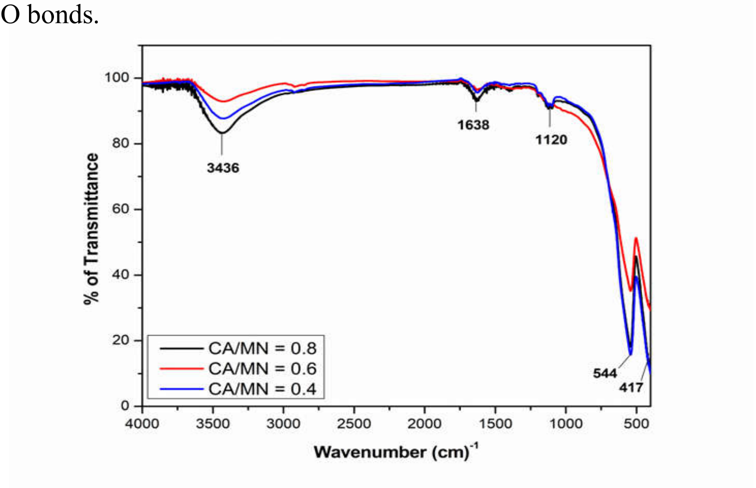

Figure 3. FT-IR analysis of Zinc ferrite nanoparticles prepared at different CA/MN ratio

3.3 Morphological Analysis

Figure 4 shows the SEM image of the zinc nitrate nanopowders prepared at different citric acid to metal nitrate ratio. Observation shows that the powder show spherical structure of uneven morphology with large agglomerates without any clear grain boundaries similar to the zinc ferrite prepared by combustion method [38, 39].

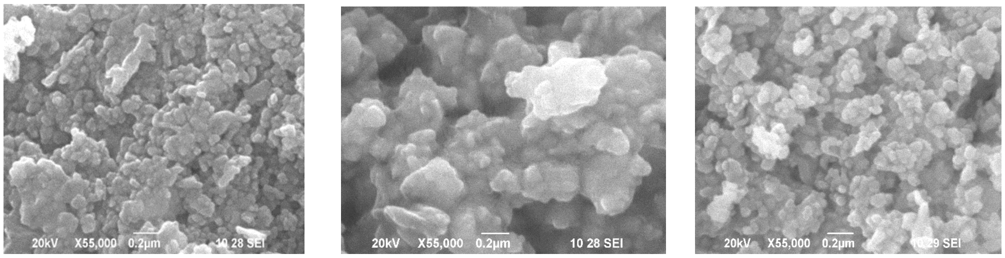

CA/MN = 0.8 CA/MN = 0.6 CA/MN = 0.4

Figure 4. SEM images of Zinc ferrite nanoparticles prepared at different CA/MN ratio

3.4 Compositional Analysis

The percentage of elements C, O, Fe and Zn in a compound can be analyzed using the EDS. The recorded EDS spectra of prepared samples are shown in the table 2 and figure 5.

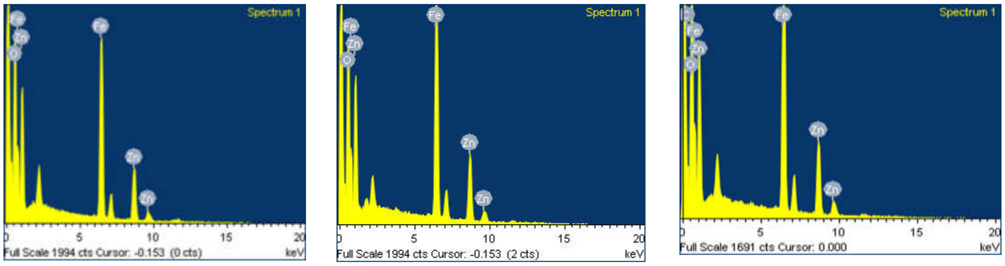

CA/MN = 0.8 CA/MN = 0.6 CA/MN = 0.4

Figure 5. Compositional analysis of Zinc ferrite nanoparticles prepared at different CA/MN ratio

Table 2. Compositional analysis of Zinc ferrite nanoparticles prepared at different CA/MN ratio

CA/MN ratio	Atomic Percentage (Weight %)			
	C (K)	O (K)	Fe (K)	Zn (K)
0.8	-	32.89	39.40	27.70
0.6	-	28.85	42.03	29.12
0.4	15.24	29.59	33.14	22.03

3.5 VSM Analysis

It is noted that magnetic properties of zinc ferrite nano powder strongly depend on its crystallinity and synthesis method. The variation of magnetization as a function of applied magnetic field for $ZnFe_2O_4$ sample at room temperature is studied using VSM and is given in figure 6. The magnetic properties such as retentivity, saturation magnetization, magnetic moment and remanence ratio and anisotropy constant is listed in the table 3. Figure 7 shows Coercivity Vs Saturation Magnetization of $ZnFe_2O_4$ with different concentration of CA/MN. The higher values of saturation magnetization are due to the non-stoichiometric structure, as it could lead to a redistribution of iron atoms in the tetrahedral sites and octahedral sites [40, 41]. The observed coercivity increases from 360 to 576 Oe when the CA/MN ratio increases. Generally, $ZnFe_2O_4$ shows the paramagnetic behavior at room temperature as reported in the literature. The observed ferromagnetism in our sample is due to the structural rearrangement which induce the changes due to the superexchange interaction in the tetrahedral and octahedral sites [42]. Also the random distribution of Zn^{2+} and Fe^{3+} at (A) and (B) sites or the defects may causes the ferromagnetic behavior [43]. The non-equilibrium distribution of Fe^{3+} ions in (A) and (B) sites may also leads to ferromagnetism [44]. Therefore, the observed magnetic properties in the present work may be due to the above mentioned facts. The anisotropic constant (k) and the magnetic moment (μ_B) are given in the table 3.

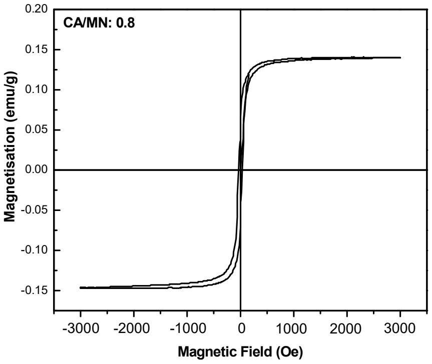

CA/MN: 0.8

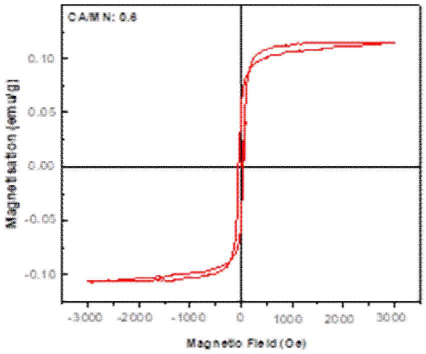

CA/MN: 0.6

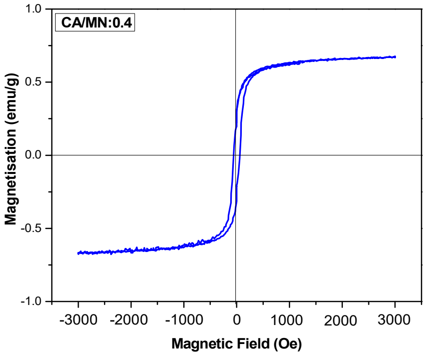

CA/MN: 0.4

Figure 6. Magnetic Parameters of the Zinc ferrite nanoparticles prepared at different CA/MN ratio

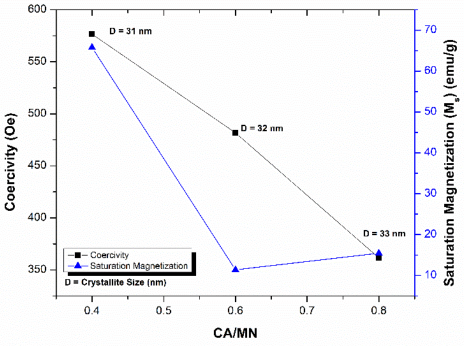

Figure 7. Coercivity Vs Saturation Magnetisation of the Zinc ferrite nanoparticles prepared at different CA/MN ratio

Table 3. Magnetic Parameters of the Zinc ferrite nanoparticles prepared at different CA/MN ratio

CA/MN ratio	Mr (emu/g)	Ms (emu/g)	Mr/Ms	K	μ_B
0.8	38	15.463	0.245748	58260.07	6.67
0.6	38.17	11.412	0.334472	57270.41	4.92
0.4	195.31	65.79	0.296869	395185.5	28.39

4. Conclusion

Zinc ferrite, a normal ferrite nanoparticle is synthesized by sol-gel technique using 0.2M zinc nitrate and 0.3M ferric nitrate as the precursor and 0.4M citric acid as the chelating agent. Structural analysis shows the variation in the grain size when the CA/MN increases from 0.8 to 0.4. The microstructural analysis shows the lattice constant and the X-ray density found to be close to the standard value for zinc ferrite nanoparticles. Zinc ferrite nanoparticle shows the agglomeration without proper boundary. The EDS spectrum shows the composition of the prepared samples. VSM analysis shows the ferromagnetic behavior of the synthesized powder. The absence of other peaks shows the pure phase of the synthesized particle.

References

[1] C. R. Martin, “Nanomaterials: a membrane-based synthetic approach”, Science, vol. 266, **(1994)** pp. 1961-1966.

[2] E. C. Snelling, “Soft ferrites: properties and applications”, Butterworth Publishing 2nd edn, London, **(1989)**

[3] D. C. Jiles, “Introduction to magnetism and magnetic materials”, Chapman and Hall 2nd edn, London, **(1991).**

[4] M. A. Willard, L. K. Kurihara, E. E. Carpenter, S. Calvin and V. G. Harris, “Chemically Prepared Magnetic Nanoparticles”, Int. Mater. Rev., vol. 49 **(2004)** pp. 125-170.

[5] O. S. Mathew and R. S. Jiang, “An Overview of the Structure and Magnetic Ferrite Nanoparticles and their Synthesis in Microemulsions”, Chem.ng. J. vol. 129 **(2007)** pp. 51-65.

[6] P. M. Prithviraj Swamy, S. Basavaraja, Arunkumar Lagashetty, N. V. Srinivas Rao, R. Nijagunappa and A. Venkataraman, “Synthesis and Characterisation of Zinc Ferrite Nanoparticles obtained by Self propagating low temperature combustion method”, Bull. Mater. Sci., vol. 34 **(2011)** pp. 1325-1330.

[7] N. Ikenaga, Y. Ohgaito, H. Matsushima, T. Suzuki, “Preparation of Zinc Ferrite in the presence of carbon material and its application to hot-gas cleaning”, Fuel, vol. 83 **(2004)** pp. 661-669.

[8] M. Atif, S. K. Hasanain, M. Nadeem, “Magnetization of Sol-Gel Prepared Zinc Ferrite Nanoparticles: Effects of Inversion and Particle Size”, Solid State Commun. vol. 138 **(2006)** pp. 416-421.

[9] De. Debasish, De. Debapriya and B. Adhikari, “Curing Characteristics and Mechanical Properties of alkali-treated grass-fiber-filled natural rubber composites and effects of bonding agent”, J. Appl. Polym. Sci., vol. 101**(2006)** pp. 3151-3160.

[10] R. Lebourgeois and C. Coillot, “Mn-Zn Ferrites for Magnetic Sensor in Space Applications”, J. Appl. Phys. vol.103 **(2008)** pp. 07E510.

[11] A. K. M. A Hossain, T. S. Biswas, T. Yanagida, H. Tanaka, H. Tabat and T. Kawai, “Investigations of Structural and Magnetic Properties of Polycrystalline $Ni_{0.50}Zn_{0.50-x}Mg_xFe_2O_4$”, Mater. Chem. Phys., vol. 120 **(2010)** pp. 461-467.

[12] F. Grasset, N. Labhsetwar, D. Li, D. C. Park, N. Saito, H. Haneda, O. Cador, T. Roisnel, S. Mornet, E. Duguet, J. Portier and J. Etourneau, “Synthesis and Magnetic Characterisation of Zinc Ferrite Nanoparticles with Different Environments: Powder, Colloidal Solution, and Zinc Ferrite-Silica Core-shell Nanoparticles”, Langmuir, vol. 18 (**2010**) pp. 8209-8216.

[13] K. Tanaka, M. Makita, Y. Shimizugawa, K. Hirao and N. Soga, “Structure and High Magnetization of Rapidly Quenched Zinc Ferrite”, J. Phys. Chem., Solids vol. 59 **(1998)** pp. 1611-1618.

[14] X. Niu and W. Du, “Preparation and Gas Sensing Properties of ZnM2O4 (M=Fe, Co, Cr)”, Sens. Actuators B Chem., vol. 99 **(2004)** pp. 405-409.

[15] J. A. Toledo-Antonio, N. Nava, M. Martínez and X. Bokhimi, “Correlation between the magnetism of non-stoichiometric zinc ferrites and their catalytic activity for oxidative dehydrogenation of 1-butene.” Appl. Catal., A Gen., vol. 234 **(2002)** pp. 137-144.

[16] J. Qiu, C. Wang and M. Gu, “Photocatalytic Properties and Optical Absorption of Zinc Ferrite nanometer films”, Mater. Sci. Eng. B, vol. 112 **(2004)** pp. 1-4.

[17] M. Kobayashi, H. Shirai and M. Nunokawa, “Measurement of Sulfur Capacity Proportional to Zinc Sulfidation on Sorbent containing Zinc Ferrite-Silica composite powder in pressurized Coal Gas.” Ind. Eng. Chem. Res., vol. 41 **(2002)** pp. 2903-2909.

[18] F. Tomás-Alonso and J. M. Palacios Latasa, “Synthesis and Surface Properties of Zinc Ferrite species in supported sorbents for coal gas desulphurization”, Fuel Process Technol., vol. 89 **(2004)** pp. 191-203.

[19] C. Yao, Q. Zeng, G. Goya, T. Torres, J. Liu, H. Wu, M. Ge, Y. Zeng, Y. Wang and J. Jiang, “$ZnFe_2O_4$ Nanocrystals: Synthesis and Magnetic Properties”, J. Phys. Chem. C, vol. 111 **(2004)** pp. 12274-12278.

[20] L. Wang, Q. Zhou, F. LiF, “Ionic Disorder and yaffet-kittel angle in nanoparticles of ZnFe2O4 prepared by sol-gel method”, Phys. Status Solidi B, vol. 241 **(2004)** pp. 377-382.

[21] A. Kundu, O. C. Upadhyay, H. Verma, “Magnetic properties of partially inverted zinc ferrite synthesized by a new co-precipitation technique using urea”, Phys. Lett. A, vol. 311 **(2003)** pp. 410-415

[22] X. Hu, P. Guan, X. Yan, “Hydrothermal synthesis of nano-meter microporous zinc ferrite”, China Particuol. vol.2 **(2004)** pp. 135-137

[23] R. Zhang, J. Huang, J. Zhao, Z. Sun and Y. Wang, “Sol-Gel Auto-Combustion Synthesis of Zinc Ferrite for moderate temperature Desulfurization”, Energy Fuels, vol. 21 **(2007)** pp. 2682-2687.

[24] B. R. Reddy, T. Sivasankar, M. Sivakumar and V. S. Moholkar, “Physical facets of ultrasonic cavitational synthesis of zinc ferrite particles”, Ultrason. Sonochem. vol.17 **(2010)** pp. 416-426

[25] B. D. Cullity, “Elements of X-Ray Diffraction”, Addison – Wesley Publishing Company Inc **(1956)**

[26] J. Smit, and H. P. J. Wijn, Ferrites. Philips Technical Library, Eindhoven 150

[27] M. K. Roy, B. Halder and H. C. Verma, “Characteristic length scales of nanosized zinc ferrite Nanotechnology”, vol. 17 **(2006)** pp. 232-237.

[28] Y. P. Sui, X. F. Huang, Z. Y. Ma, W. Li, F. Qiao and K. J. Chen, “The effect of thermal annealing on crystallization in a Si:H/SiO$_2$ multilayers by using layer by layer plasma oxidation. J. Phys. Condens. Matter., vol. 15 **(2011)** pp. 5793-5800.

[29] Zehui Jiang, Zhijia Liu, Benhua Fei, Zhiyong Cai, Yan Yu and Xing’e Liu, “The pyrolysis characteristics of moso bamboo”,J. Anal. Appl. Pyrolysis, vol. 91 **(2011)** pp. 48-52

[30] A. Pandit, A. R. Shitre, D. R. Shengule, K. M. Jadhav, “Magnetic and Dielectric properties of Mg1+xMnx, Fe2-2x, O4 ferrite system”, J. Mater. Sci., vol. 40 **(2005)** pp. 423-428.

[31] A. Muhammad and A. Maqsood, “Structural, Electrical and Magnetic Properties of Cu$_{1-x}$Zn$_x$Fe$_2$O$_4$ ferrites (0<x<1)”, J. Alloy. Com. vol. 460 **(2008)** pp. 54-59.

[32] N. Zotov, K. Petrov and M. Dimitrova Pankova, “Infrared spectra of Cu(II)-Co(II) mixed hydroxide nitrates”, J. Phys. Chem. Solids, vol. 51 **(1990)** pp. 1199-1205.

[33] P. Laokul, V. Amornkitbamrung, S. Seraphin and S. Maensiri, “Characterization and magnetic properties of nanocrystalline CuFe$_2$O$_4$ powders prepared by the Aloe Vera extract solution”, Curr. Appl. Phys. vol. 11 **(2011)** pp. 101-108.

[34] M. I. Loría-Bastarrachea, W. Herrera-Kao, J. V. Cauich-Rodríguez, J. M. Cervantes-Uc, H. Va’zquez-Torres and A. A. Vila-Ortega, “A TG/FTIR Study on the Thermal degradation of Poly(vinyl pyrrolidone)”, J. Therm. Anal. Calorim. vol. 104 **(2010)** pp. 737-742

[35] C.N. R. Rao, Chemical applications of infrared spectroscopy (New York and London: Academic Press) **(1963)**

[36] G. V. S. Rao, C.N.R. Rao and J. R. Ferraro, “Infrared and Electronic Spectra of Rare Earth Perovskites: Ortho-Chromites, -Manganites and Ferrites”, Appl. Spectrosc. vol. 24 **(1970)** pp. 436-445.

[37] R. D Waldron, “Infrared Spectra of Ferrites”, Phys. Rev. vol. 99 **(1995)** pp. 1727-1735.

[38] T. Striker and J. A. Ruud, “Effect of Fuel choice on the aqueous combustion synthesis of lanthanum ferrite and lanthanum manganite”, J. Am. Ceram. Soc. vol. 93 **(2010)** pp. -2629.

[39] H. Kavas, N. Kasapogˇlu, A. Baykal A, and Ko¨seogˇlu Y, “Characterization of NiFe2O4 nanoparticles synthesized by various methods, “Chem. Papers, vol. 63 **(2009)** pp. 450-455.

[40] J. Wang, K. Zhang, Z.M. Peng and Q. W. Chen, “Magnetic Properties improvement in Fe3O4 nanoparticles grown under magnetic fields”, Journal of Crystal Growth, vol. 266 **(2004)** pp. 500-504.

[41] A. S. Teja and P.Y. Koh P Y, “Synthesis, Properties and Application of Magnetic Iron Oxide in Nanoparticles. Progress in Crystal Growth and Characterization of Materials, vol. 55 **(2009)** pp. 22-45.

[42] N. M. Deraz and A. Alarifi, “Synthesis and Physicochemical Properties of Nanomagnetic Zinc Ferrite System”, International Journal of Electrochemical Science, vol. 7 **(2012)** pp. 3798-3808

[43] A. T. Raghavender, N. Biliskov and Z. Skoko, “XRD and IR analysis of nanocrystalline Ni–Zn ferrite synthesized by the sol–gel method”, Materials Letters, vol. 65 **(2011)** pp. 677

[44] M. Bohra, S. Prasad, N. Kumar, D. Misra, S. Sahoo, N. Venkataramani and R. Krishnana, “Large Room Temperature Magnetization in nanocrystalline zinc ferrite thin films”, Applied Physics Letters, vol. 88 **(2006)** pp. 262506-3.